Pure appl. geophys. 154 (1999) 365–396
0033–4553/99/020365–32 $ 1.50 + 0.20/0

Pure and Applied Geophysics

Numerical Investigation of the Somali Jet Interaction with the Western Ghat Mountains

YIHUA WU,[1] SETHU RAMAN[1] and U. C. MOHANTY[2]

Abstract—Several major features of the interaction of the Somali jet with the Western Ghat Mountains have been observed. These include a pressure ridge, strong vertical motions, and occurrences of highly reflective cloud and heavy rainfall rates along the west coast of India. A triple nested regional weather prediction model has been used to investigate the dynamic interaction between the Somali jet and the Western Ghat Mountains. Two numerical experiments were conducted; one with the topography of western India and the other without. In the experiment without topography, the Western Ghat Mountains were removed from the innermost domain. The results for the innermost domain in the two experiments were analyzed and compared. The results from the simulation with topography captured several of the observed features of the Somali jet interaction with the Western Ghat Mountains. The simulation without topography failed to reveal these features. The results suggest that the blocking effect of the Western Ghats plays an important role in the prediction of the rainfall over the west coast of India.

Key words: Numerical investigation, Somali jet, the Western Ghat.

1. Introduction

The Somali low-level jet (SLLJ) is a major component of the southwest summer monsoon. This moist-laden high-speed current, forming on the western boundary of a broad cross-equatorial current, is shown to flow intermittently from the vicinity of Mauritius through Madagascar, Kenya, eastern Ethiopia, and Somalia. It then crosses the Arabian Sea to reach the west coast of India and beyond and transports moisture to the Indian subcontinent during the southwest monsoon. Standing on the west coast of India about 50 km inland, the Western Ghat Mountains (WGM) are about 1600 km long in the north–south direction, 500 km wide in the west–east direction, and 800 m high on the average with individual peaks reaching 1100 m.

[1] Department of Marine, Earth and Atmospheric Sciences, North Carolina State University, Raleigh, NC 27695-8208, USA.
[2] Center for Atmospheric Sciences, Institute of Technology, New Delhi, 110016, India.

The orientation of the WGM is more or less perpendicular to the mean SLLJ direction. The SLLJ, over and around the big changes in land surface elevation in a rotating stratified fluid, represents a classical problem in meteorology and oceanography.

Several investigators have studied the interaction of the SLLJ with the WGM. (1) Results indicated that the west coast of India is a region with substantial rainfall during the southwest monsoon. The analysis by KRISHNAMURTI *et al.* (1983) shows that maximum rainfall rate along the west coast of India could be as high as about 200 mm d^{-1}. During the period of July 12–14, 1988, a rainfall rate exceeding 100 mm d^{-1} was observed along the west coast. Studies of the physics of orographic convective precipitation over the western coast of India have been conducted by several investigators. SARKER *et al.* (1978) applied their two-dimensional model for orographic rainfall caused by the Western Ghats. During the active monsoon situations, they found the peak in rainfall distribution to be purely an orographic effect. However, SMITH and LIN's (1983) simulation indicates that the latent heating induces upward motion over the heating area upwind. Latent heating also strengthens the orographic lifting of potentially unstable air. Their study suggests that the latent heating is an important factor for the occurrence of rainfall over the west coast of India. OGURA and YOSHIZAKI (1988) conducted several numerical experiments using a two-dimensional compressible moist cloud model to study the physics underlying orographic-convective precipitation over the west coast of India. Their results indicate that in order to account for the observed features of rainfall over the area, two factors are essential. These are the strongly sheared environment and fluxes of latent heat from the ocean. (2) An eastward increase of surface pressure over the Arabian Sea is often observed during the summer monsoon season (VAN DE BOOGAARD, 1977). The axis of the pressure ridge is either coincident or just upstream of the ridge line of the WGM. A pressure ridge was also observed along the west coast of India on the 12th, 13th and 14th of July 1988. This positive pressure perturbation could be the result of adiabatic cooling of the low-level air lifted by the upstream blocking effect of the mountains. To investigate the interaction of Somali jet with the WGM, GROSSMAN and DURRAN (1984) conducted a numerical simulation using a two-dimensional, analytical, nonlinear model. Their simulation showed a decrease in the atmospheric boundary layer wind speed, a pressure rise in the subcloud layer and an increase in large-scale upward vertical velocity. (3) GROSSMAN and DURRAN (1984) also found that highly reflective clouds occur just upstream of the WGM from June through August. Occurrence of these clouds could be due to the lifting effect of the mountains. These results suggest that the major influence of the WGM on the SLLJ is upstream blocking.

In this paper, we will use a nested mesoscale model to investigate this interaction, to show its major features, and to reveal its mechanisms. A summary of summer monsoon synoptic flow and rainfall distribution over the Indian subconti-

nent for the period, July 12–24, 1988 is given in Section 2. Section 3 contains a brief description of the NRL/NCSU regional weather prediction model. The model setup and the numerical experiment design are given in Section 4. Simulation results from two numerical experiments and corresponding discussions are given in Sections 5 and 6.

2. Synoptic Overview

Indian southwest monsoon has been studied for several decades (DAS, 1972; RAMAGE, 1971; FEIN and STEPHENS, 1987). There are several semi-permanent features associated with the summer monsoon circulations. They are the monsoon trough over the northern Indian subcontinent, the SLLJ over the Arabian Sea and the tropical easterly jet in the upper troposphere. Usually, the monsoon trough is located along the Gangetic Plains with an orientation from northwest to southeast. During the active monsoon period, the monsoon trough is large with one end over the heat low in northwest Rajasthan and the other end over the Bay of Bengal, crossing the entire northern region of India. Low pressure systems often develop over the Bay of Bengal, intensifying into monsoon depressions. Thereafter they move over the land along the monsoon trough, causing considerable rainfall over India. Throughout the summer monsoon season, the SLLJ across the Arabian Sea approaches India with a speed of about 15 m s^{-1} at 850 mb. The direction is more or less perpendicular to the longer axis of the WGM. The interaction of the SLLJ with the WGM enhances the rainfall along the west coast of India. Air flow is reversed in the upper troposphere, blowing from the east. This shear environment presents conditions conducive for the creation of disturbances in both lower and upper tropospheres. These disturbances play an important role in modulating rainfall in this region. The geography locations of the Arabian Sea, Bay of Bengal, Rajasthan, the WGM and the Gangetic Plains are shown in Figure 1.

During the period from July 12 to 14 of 1988, the monsoon was moderately active over the Indian subcontinent. Figure 2 shows the observed mean sea level pressure (MSLP) fields at 0000 UTC 12, 13 and 14 of July. At 0000 UTC 12 July (Fig. 2a), a heat low with a minimum pressure less than 994 mb was located over the 28 N and 69 E. A weak monsoon trough developed over the northern region of India. A pressure ridge over the west coast of India is also apparent. By the time of 0000 UTC 13 July (Fig. 2b), the heat low became deeper, with a minimum pressure less than 992 mb. The monsoon trough over northern India was now stronger than that at the previous time. The pressure ridge over the west coast of India changed minimally. By the time of 0000 UTC 14 July (Fig. 2c), the intensity of the heat low was about the same as the previous time; however, its center had moved by about 100 km to the south. The monsoon

trough over northern India became stronger. The pressure ridge over the west coast of India also increased in magnitude. For the three days, the low-level air blew from the southwest over the Arabian Sea, however the direction changed to northwest after arriving at the west coast of India.

The observed cumulative rainfall distribution (mm day^{-1}) ending at 0300 UTC on 13 and 14 July 1988 is shown in Figures 3a and 3b, respectively. The rainfall occurred mainly over two regions: one is the central to the northern parts of India; the other is a region along the west coast of India. The maximum rainfall rate over the central and northern regions of India as well as over the west coast of India was about 100 to 140 mm day^{-1} for the period. Rainfalls over the central and northern regions of India were caused by a monsoon low pressure system located over northeast India. The rainfall over the west coast of India was due to the orographic

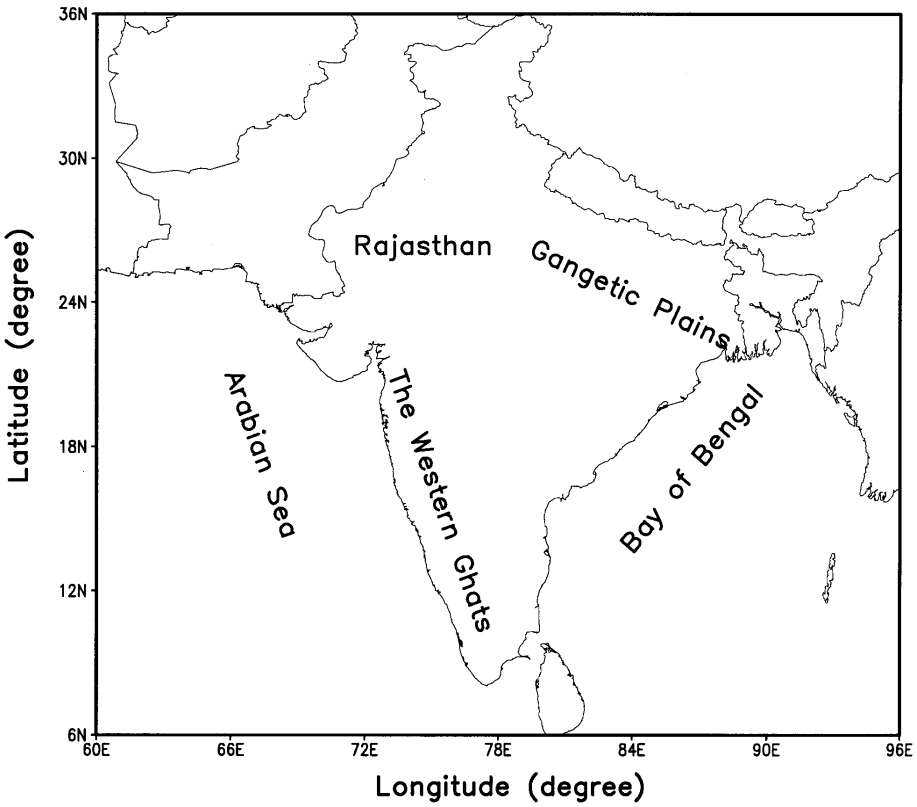

Figure 1
Geography of India and its surrounding regions.

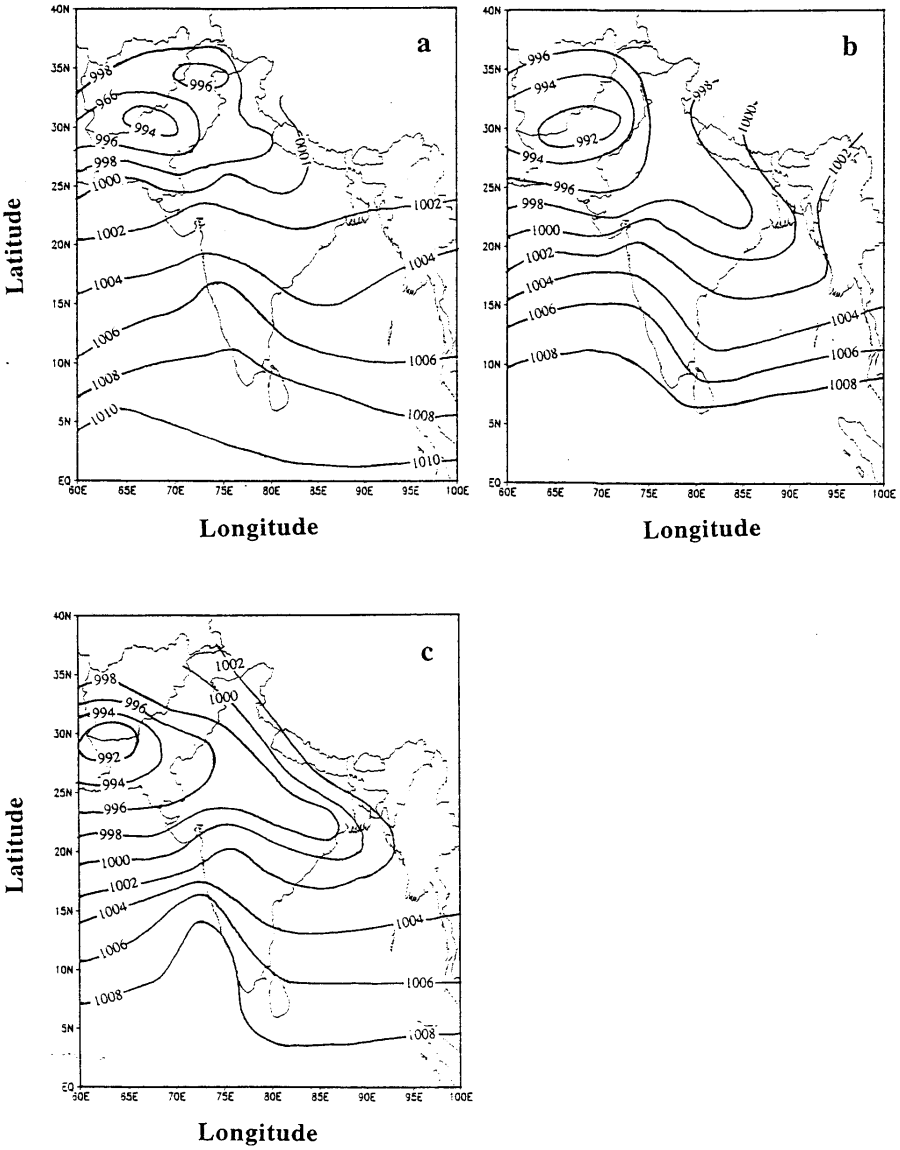

Figure 2
The mean sea-level pressure (mb) observed at 0000 UTC. (a) 12 July 1988, (b) 13 July 1988, (c) 14 July 1988.

lifting and associated convection. Thus the monsoon activities during this period provide an excellent case with which to study the interaction of the SLLJ with the WGM.

3. Model Description

The model used in this study is a modified version of the regional weather prediction model originally developed at the Naval Research Laboratory and North Carolina State University by MADALA *et al.* (1987). This is a primitive equation model. The continuous governing equations are written in flux form. This model is written in the pressure-based, terrain-following σ vertical coordinate system which means that the lower grid levels follow the terrain while the upper surface is flat. The intermediate levels progressively flatten as the pressure decreases toward the chosen top pressure. A staggered grid network (Arakawa C-grid) is used for the horizontal difference. The grid includes the surface pressure (p_s), specific humidity (q), temperature (T), geopotential (ϕ) and vertical velocity (ω). They are specified at the same horizontal points and have zonal and meridional winds (u and v) between them.

This version contains a capability of multiple nesting with up to three domains running simultaneously and one-way interacting. The nesting ratio is 3:1, i.e., every third grid in a subdomain is collocated with that in its mother domain. One-way interacting ensures that the boundary values for a subdomain are specified by the interior grid points of its mother domain, while no feedback to the mother domain occurs. The grid size and time step are three times less for a subdomain than for its mother domain. Lateral boundary conditions for the three domains are provided using the DAVIES scheme (1976, 1983). For any independent variable X, it can be expressed as: $X = (1-a)X_m + aX_b$, where the subscript m represents model-com-

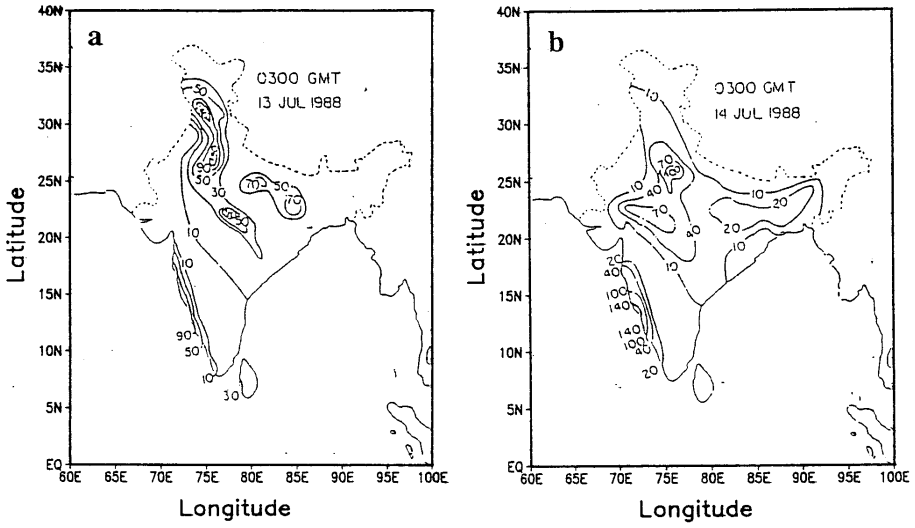

Figure 3
Accumulated rainfall (mm d^{-1}) ending at 0300 UTC. (a) 13 July 1988, (b) 14 July 1988.

puted values and subscript b denotes the boundary values obtained either from observations or from a coarser version of the model. The coefficient, a, ranges from 0 to unity, depending on the location of grid in the boundary zone.

In the model, the boundary layer is divided into the surface layer and the mixed layer. The surface layer is parameterized based on similarity theory (MONIN and YAGLOM, 1971), and the mixed layer is parameterized using the $E-\varepsilon$ closure scheme (HOLT and RAMAN, 1988). The surface physics calculations are performed using the NOILHAM and PLANTON (1989) soil-vegetation parameterization scheme which is simple but preserves the representation of the physics controlling the energy and water budgets at the soil-vegetation-atmosphere interface.

The parameterization of convective precipitation used in this model is a modified Kuo scheme (KUO, 1974; ANTHES, 1977) which pertains only to columns in which the atmosphere is conditionally unstable and in which the total horizontal convergence exceeds a critical value. A fraction of the total moisture convergence in a column is condensed in cumulus convection and is precipitated out depending on the mean columnar relative humidity. The remainder is retained in the column to increase the humidity of the column and to offset the drying effects of the vertical eddy flux terms. Nonconvective precipitation occurs in the model when super-saturation is reached on the resolvable scale. Excess moisture precipitates into lower model layers and evaporates or falls to the surface, depending upon the degree of saturation at those levels.

A split-explicit method is used for time integration in this model. This method allows utilization of different time steps for the slow-moving Rossby modes and for the fast-moving gravity modes in the prognostic equations. A smaller time step is used for the first and second fast-moving gravity modes, while a larger time step is used for all other modes. More details about this method as well as this model are given by MADALA *et al.* (1987), HOLT *et al.* (1990) and SASHEGYI and MADALA (1993).

4. Model Setup and Experiments

The model domains used for this study are displayed in Figure 4. The coarse domain (CD) is of 8580 km × 9900 km size (61 × 53 grid points) and covers most of the monsoon region. The middle domain (MD) size is 5280 km × 3960 km (97 × 73 grid points) and encompasses most of the Indian subcontinent and its surrounding oceans. The innermost fine domain (FD) covers the western coastal region of India and the eastern Arabian Sea, sized at 1320 km × 1980 km (109 × 73 grid points). Horizontal grid resolutions in the CD, the MD and the FD are 1.5°, 0.5° and 0.17° latitude/longitude, respectively. The vertical structure includes 16 σ levels with the model top at 50 mb. Eight levels are within the lowest 2 km (σ greater than 0.8) with finer resolution at lower levels, and eight equally spaced levels ($\Delta\sigma = 0.1$) above 2 km.

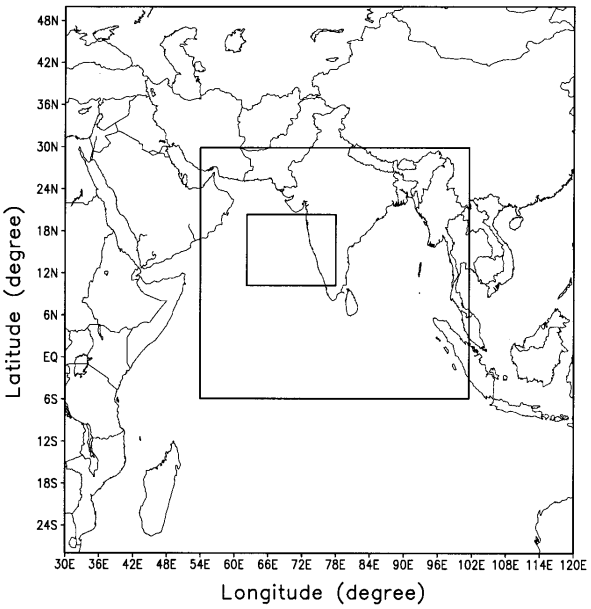

Figure 4
Physical domains used in the model.

The model orography was obtained from the Navy 10′ global topography. The topography for the CD, the MD, and the FD is shown in Figure 5. It can be seen that peaks of the WGM are closer to the west coast of India in the finer domains as compared to the coarser ones. The model topography captures the features of the WGM better as the domain becomes finer. However, even the model terrain in the FD does not reach the true crest height of the mountains and does not fully capture the steepness of the orography. Model sea-surface temperatures (SST) were obtained from the 1 degree resolution global climatological values on a 10-year average for the month of July. Meteorological initial conditions (wind components, temperature, water vapor mixing ratio and surface pressure) for the model simulation were interpolated from the European Center for Medium-Range Weather Forecasting (ECMWF) operational analysis over a horizontal resolution of 1.875° latitude/longitude. Lateral boundary conditions (X_b) for the CD grid points are obtained through a linear interpolation in time step from the ECMWF analyses. On the other hand, lateral boundary conditions for the MD and the FD were obtained from the corresponding mother domain. At the model bottom and top, the boundary condition for vertical velocity (ω) is assumed zero.

Two numerical experiments were conducted. In the control experiment (hereafter referred to as CNTRL), the topography was incorporated in the three domains. In the second experiment (hereafter referred to as NOTOP), the topogra-

phy was removed from the FD. Numerical simulations were performed for 48 hours, starting from 1200 UTC 12 July 1988. The simulated results at model forecast hours 12 h and 36 h which correspond to 0000 UTC (local time 05:30 am) July 13 and 14, 1988 were analyzed to reveal salient features produced by the interaction of the SLLJ with the WGM. Only the results simulated over the FD are presented and discussed in this paper.

5. Results of the Control Run

In this experiment (CNTRL), the orography obtained from the Navy 10′ global topography was incorporated in the three domains. To show the features of the SLLJ interaction with the WGM, simulated results of mean sea-level pressure, wind speeds, latent heat flux, vertical motion and rainfall are discussed below.

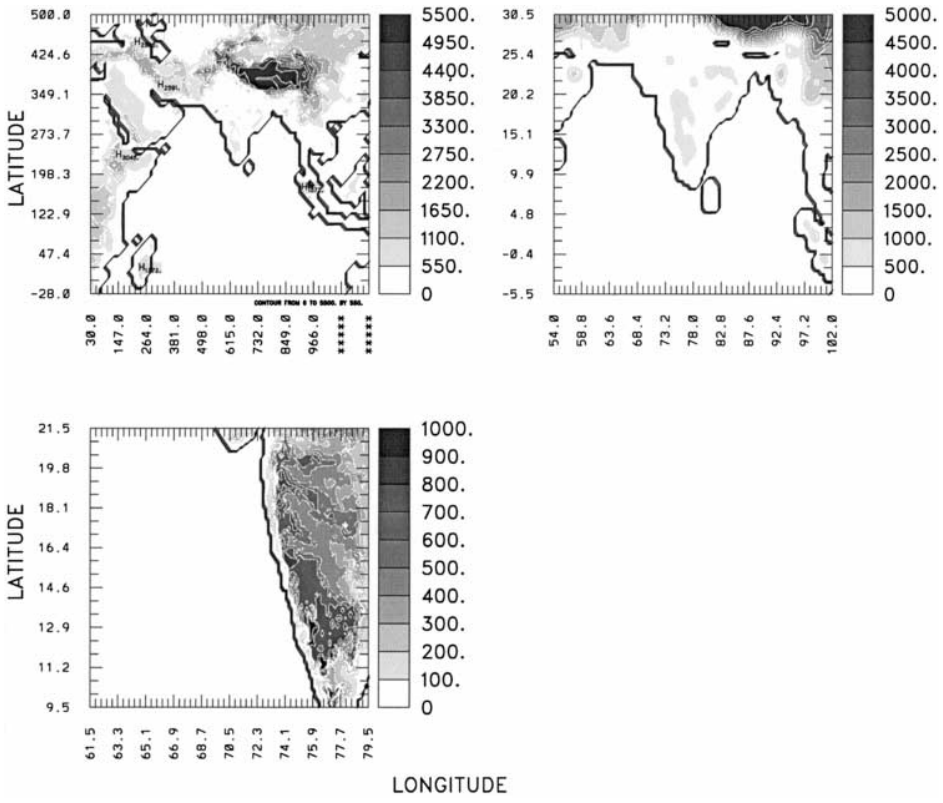

Figure 5
Topography (m) in the model. (a) Topography in coarse domain, (b) topography in middle domain, (c) topography in fine domain.

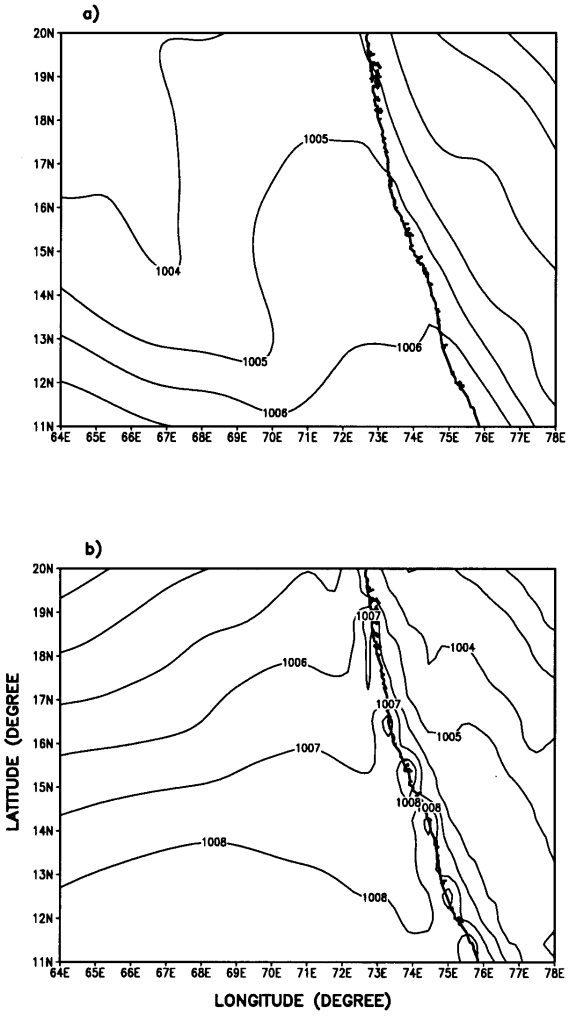

Figure 6
Simulated mean sea-level pressure (mb) in the CNTRL. (a) 12 h, (b) 36 h.

5.1. The Pressure Ridge over the West Coast of India

The interaction of the SLLJ with the WGM greatly modifies mean sea-level pressure. Figure 6 illustrates the simulated mean sea-level pressures (MSLP) at 12 h and 36 h. At 12 h (Fig. 6a), a strong pressure gradient is predicted west of the mountains. A pressure ridge is located just off the west coast of India. The difference of the MSP between 73°E and 78°E is about 5 mb. Compared with the analysis in Figure 2b, the predicted pressure ridge is stronger. The model produced a strong trough at 67°E while the analysis reveals a weak pressure ridge over this

region. The pressure distribution simulated at 36 h (Fig. 6b) is comparable to that in Figure 1c. The pressure ridge is considerably narrower than that at the previous time. The difference of the MSP between 74°E and 78°E is about 4 mb. This tendency indicates that the pressure ridge at 36 h is at the stage of deformation. A pressure trough develops in the region, possibly due to the continuous heavy rainfall in this region. The pressure ridge along the west coast of India is mainly due to the blocking effect of the WGM. As the low-level westerly flow is blocked by the WGM, air mass accumulating on the west side of the barrier is lifted upward. Lifting causes mid-level adiabatic cooling which in turn creates a deep layer of cool and dense air. This increases the low-level pressure hydrostatically. Consequently, a high pressure region is created. As shown later in a numerical experiment with no topography (NOTOP), such a pressure ridge is absent from the simulation when topography is removed from the fine domain. The blocking effect is also apparent in the wind field, as will be discussed in the next section.

5.2. The Deceleration and Deflection of the SLLJ

Both low- and upper-level winds are greatly modified by the effects of the WGM. Wind fields predicted at 12 h and 36 h are given in Figures 7 and 8. Panels *a* and *b* in these two figures are the pressure-longitude cross sections of *u* and *v* components, respectively, while panels *c* and *d* are the distributions of horizontal wind speeds and the streamlines at 850 mb. Compared with the *V* component (Figs. 7b and 8b), it is apparent that the *U* component (Figs. 7a and 8a) contributes most to the horizontal wind speed. The east–west *U* component has positive values below 500 mb, but negative values above 500 mb, indicating a wind reversal zone around 500 mb. The structure of the SLLJ is clearly seen in the *U* component contours. At 12 h, the *U* component has its maximum positive value larger than 18 m s^{-1} at 900 mb, at the core of SLLJ. The SLLJ extended from the western Arabian Sea and reached as far as 73°E (Fig. 7a). As shown in Figure 7a, *U* component values below 800 mb decreased as SLLJ approached the west coast of India, showing the blocking effect of the WGM. Although the *V* component (Fig. 7b) is not an important factor for horizontal wind speeds, it does indicate the blocking and deflecting effects of the WGM. As shown in Figure 7b, the value of the *V* component is positive (southerly) west of 69°E and becomes negative (northerly) east of 69°E, and the negative value increased to its maximum at 72°E, indicating the change in wind direction. The blocking and deflecting effects of the WGM are also apparent in the horizontal wind speeds and streamlines at 900 mb (Figs. 7c and 7d). While the maximum wind speed decreased from 20 m s^{-1} at 65°E to 10 m s^{-1} at 75°E (Fig. 7c), the direction of the horizontal wind speeds turned from the southwest to northwest over the Arabian Sea (Fig. 7d). The minimum horizontal wind speed at 900 mb is located in a region along the west coast with a value of 10 m s^{-1} (Fig. 7c). The blocking and deflecting effects are also apparent in

wind fields at 36 h. As shown in Figure 8a, the maximum U component values below 450 mb are located at the western boundary of the domain (larger than 24 m s^{-1}). As the SLLJ approaches the west coast of India, the U component magnitude decreases to about 15 m s^{-1}. The height of the SLLJ core is around 900 mb. The V component (Fig. 8b) also changes from a positive sign (southerly) to a negative sign (northerly) at about 71°E, indicating the change in wind direction. The maximum horizontal wind speeds of the SLLJ at 900 mb (Fig. 8c) exceed 26 m s^{-1}, stronger than the values at 12 h. As the jet approaches the west coast of India its horizontal wind speeds decreased. The difference in wind speeds between

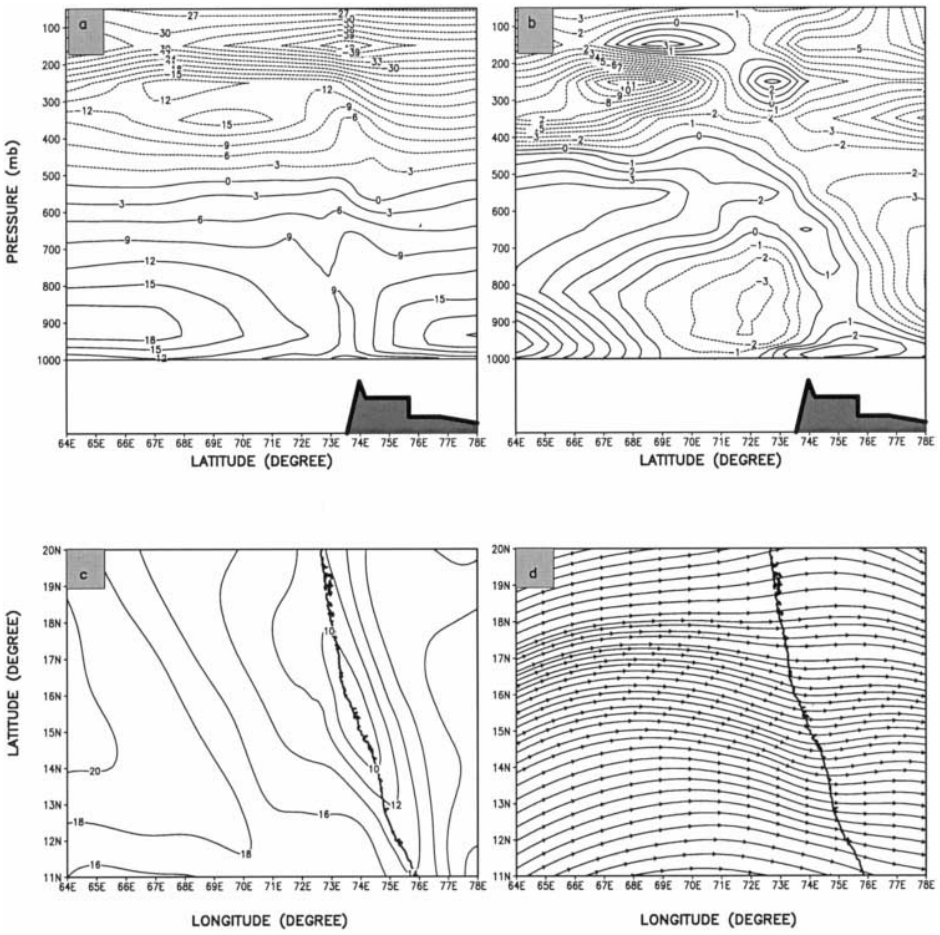

Figure 7
Simulated wind fields (m s^{-1}) in the CNTRL at 12 h. (a) Longitude-height cross section of U component at 16°N, (b) longitude-height cross section of V component at 16°N, (c) horizontal wind speed at 900 mb, (d) streamlines at 900 mb.

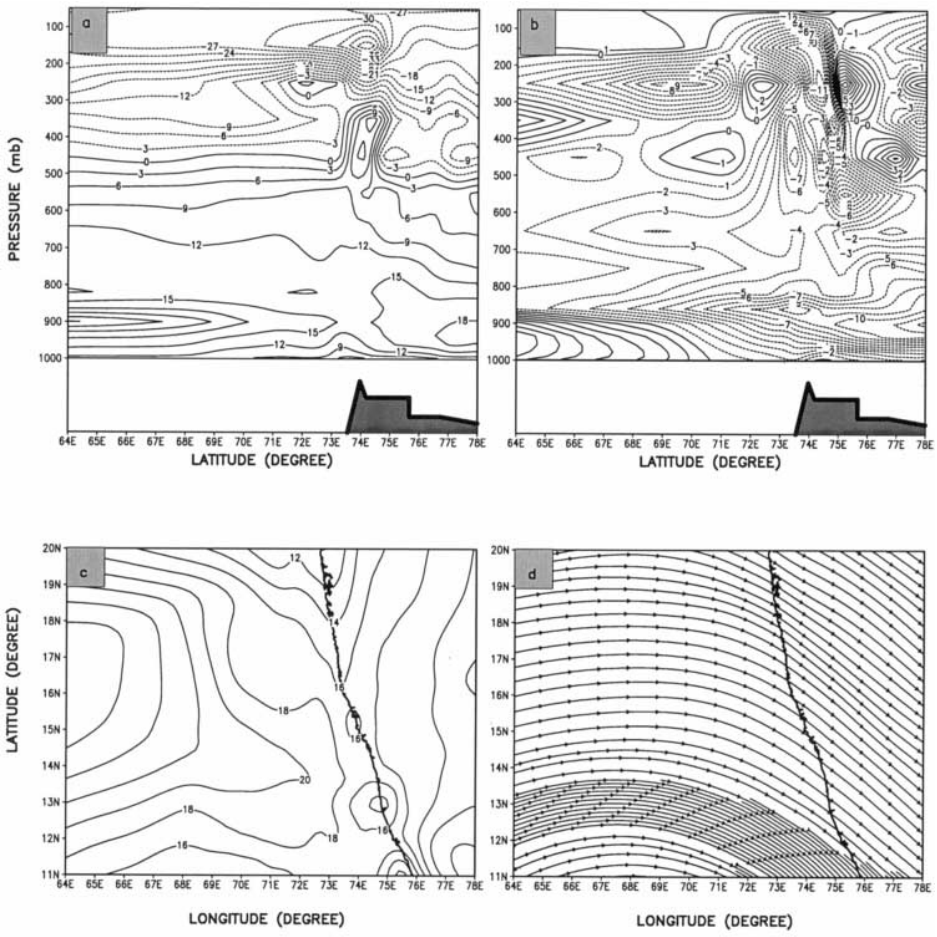

Figure 8
Simulated wind fields (m s^{-1}) in the CNTRL at 36 h. (a) Longitude-height cross section of U component at 16°N, (b) longitude-height cross section of V component at 16°N, (c) horizontal wind speed at 900 mb, (d) streamlines at 900 mb.

65°E and 75°E is about 10 m s^{-1} (Fig. 8c). The minimum horizontal wind speed at 900 mb is also located along the west coast. The simulated results at both 12 h and 36 h indicate that due to the blocking and deflecting effects of the WGM, there is a decrease in the speed of the SLLJ and a change in its direction from west to northwest. There are four possible explanations for this. The first is the development of a monsoon depression over eastern India. The second is the Coriolis effect. The third is the dynamics in the flow generated by the large thermal contrast between the Arabian Sea and the peninsular India. The fourth is the blocking and deflecting effects of the WGM. A comparison of the CNTRL run with the NOTOP

run to be presented in Section 7 indicates that the speed reduction and direction change of the SLLJ is mainly caused by the blocking and defecting effects of the WGM.

Another important feature shown in Figures 7 and 8 is the Upper Level Tropical Easterly Jet (ULTEJ), one of the semi-permanent features of the Asian summer monsoon circulation. Generally, in the upper troposphere, this jet extends from Indochina to the west coast of Africa and attains its maximum speed near latitudes 5°–10°N over the Arabian Sea (KRISHNAMURTI, 1971). This jet has been observed to exhibit interannual variations due to anomalously warm surface water appearing over the eastern and central equatorial Pacific (CHEN and LOON, 1987). At 12 h (Fig. 7a), the jet reaches a height of 150 mb with maximum wind speed exceeding 40 m s^{-1}. At 36 h (Fig. 8), the jet is slightly weaker. At both 12 h and 36 h, location of the maximum speeds of the easterly jet are just above the WGM. The reversal zone between the low-level and the upper-level jets for 12 h and 36 h is at 500 mb and 450 mb, respectively.

5.3. Latent Heat Fluxes over the Arabian Sea

Simulated latent heat fluxes at 12 h and 36 h are given in Figure 9. The simulated latent heat fluxes appear to be consistent with the observations (HOLT and RAMAN, 1986, 1987). Latent heat flux distributions over the land are different for the two hours. At 12 h (Fig. 9a), the distribution is centered with a maximum of 150 W m^{-2} over the northeast region of the domain. At 36 h (Fig. 9b), latent heat flux over the land is of the order of 30 W m^{-2}. Latent heat flux distributions over the Arabian Sea are similar at both 12 h and 36 h, with a maximum value of 210 W m^{-2} over the northwest corner of the domain, decreasing toward the southeast. Along the west coast of India, latent heat fluxes are of the order of 30–60 W m^{-2} with a significant horizontal gradient. However, at 36 h (Fig. 9b), location of the maximum over the Arabian Sea is closer to the west coast of India, producing a stronger gradient along the west coast. Latent heat flux from the Arabian Sea is believed to play an important role in the rainfall along the west coast. According to SMITH and LIN (1983) and SMITH (1985), the latent heating more strongly influences the flow upstream of the heating than that of the mountain. However, a careful comparison of the simulation results of the CNTRL run with the NOTOP run in this study suggests that the WGM may be more important than the latent heating from the ocean to the vertical motions and rainfall along the west coast of India.

5.4. Vertical Motions over the West Coast of India

Simulated vertical velocities (cm s^{-1}) at 12 h and 36 h are shown in Figures 10 and 11, respectively. Panels *a* and *b* in these two figures are the height–latitude

cross section at 76°E and height–longitude cross section at 16°N, respectively while panel *c* is the horizontal distribution of the simulated vertical velocity near the surface. At 12 h, strong upward motions between 11°N and 17°N were simulated with a maximum of about 90 cm s^{-1} near the surface (Fig. 10a). The upward motion reached as high as 650 mb. Downward motion was predicted around 18°N. The height–longitude cross section (Fig. 10b) demonstrates that upward motion occurred over the top of the mountain (around 74°E) and a downward motion east of the mountain (downstream of motion). The maximum speed of the upward

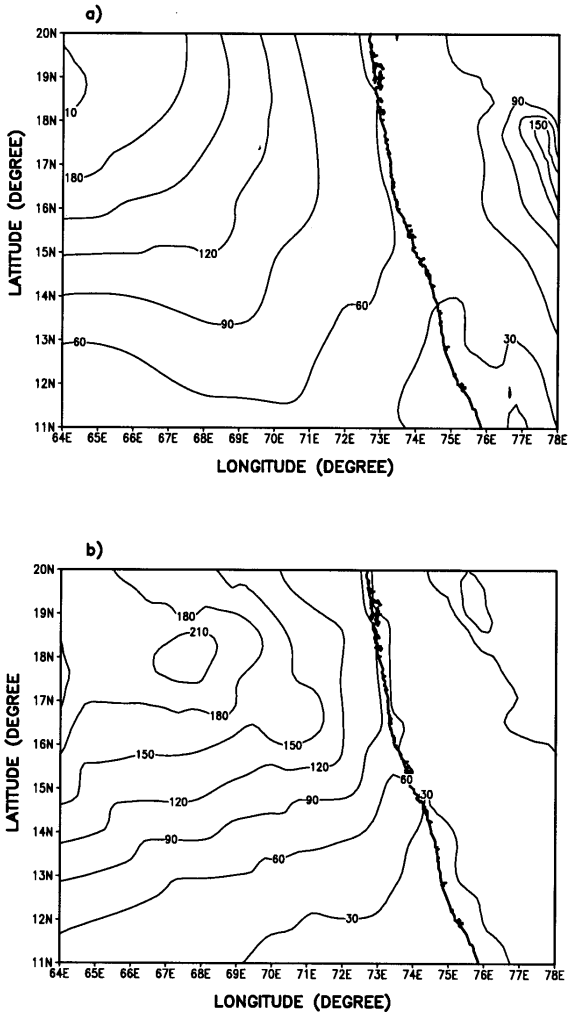

Figure 9
Simulated latent heat flux (W m^{-2}) in the CNTRL. (a) 12 h, (b) 36 h.

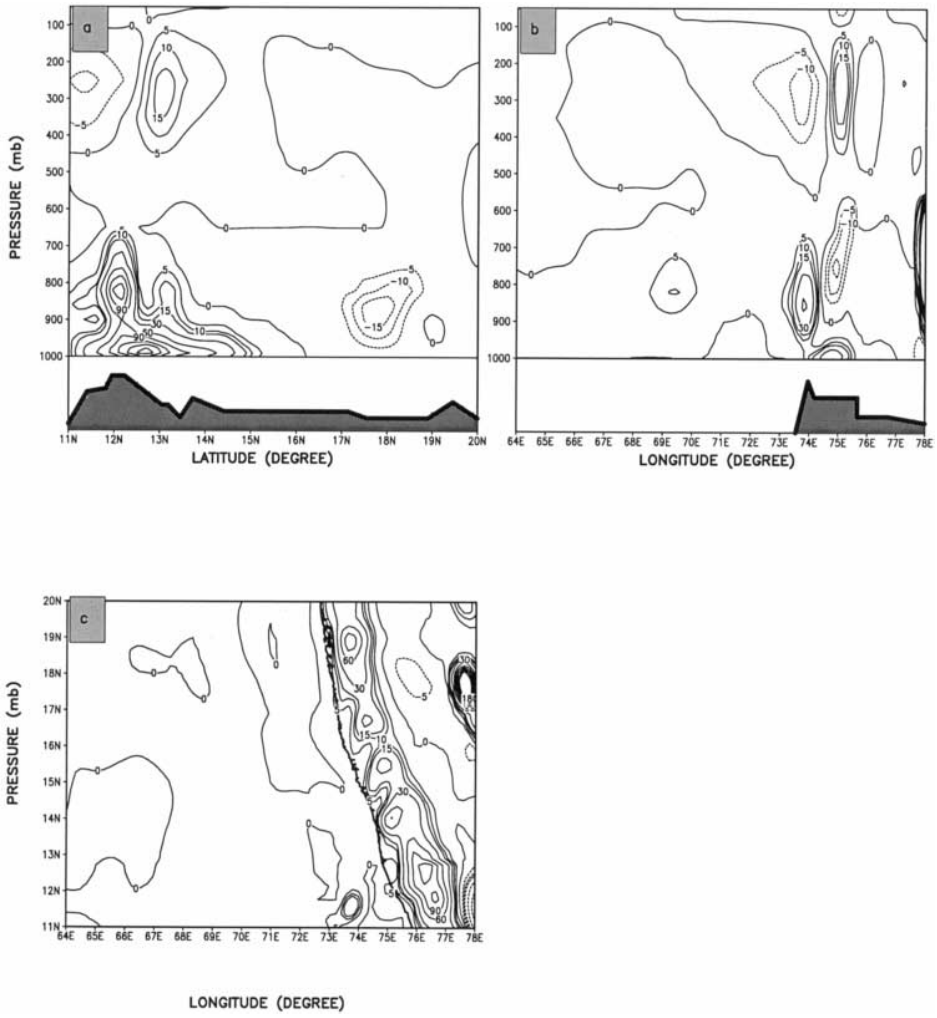

Figure 10
Simulated vertical velocities (cm s^{-1}) in the CNTRL at 12 h. (a) Latitude-height cross section at 76°E, (b) longitude-height cross section at 16°N, (c) horizontal distribution near the surface.

motion is about 45 cm s^{-1} while the maximum speed of the downward motion is about 15 cm s^{-1}. Figure 10c shows that there is very strong upward motion near the surface along with WGM. The maximum upward velocity exceeds 180 cm s^{-1}. The vertical velocity distribution pattern at 36 h (Fig. 11) is very similar to that described above. However, as shown in Figure 11a, the upward motion between 11°N and 17°N is below 800 mb with most of it occurring below 900 mb. The

downward motion between 17°N and 20°N is stronger than previously. The height–longitude cross section (Fig. 11b) indicates that there are two upward motion regions below the 400 mb level. One is the region around 73°E, well off shore and the other is over the mountain top. Figure 11c shows the clear-surface upward motion along the west coast of India. The maximum vertical velocity near the surface exceeds 110 cm s^{-1}.

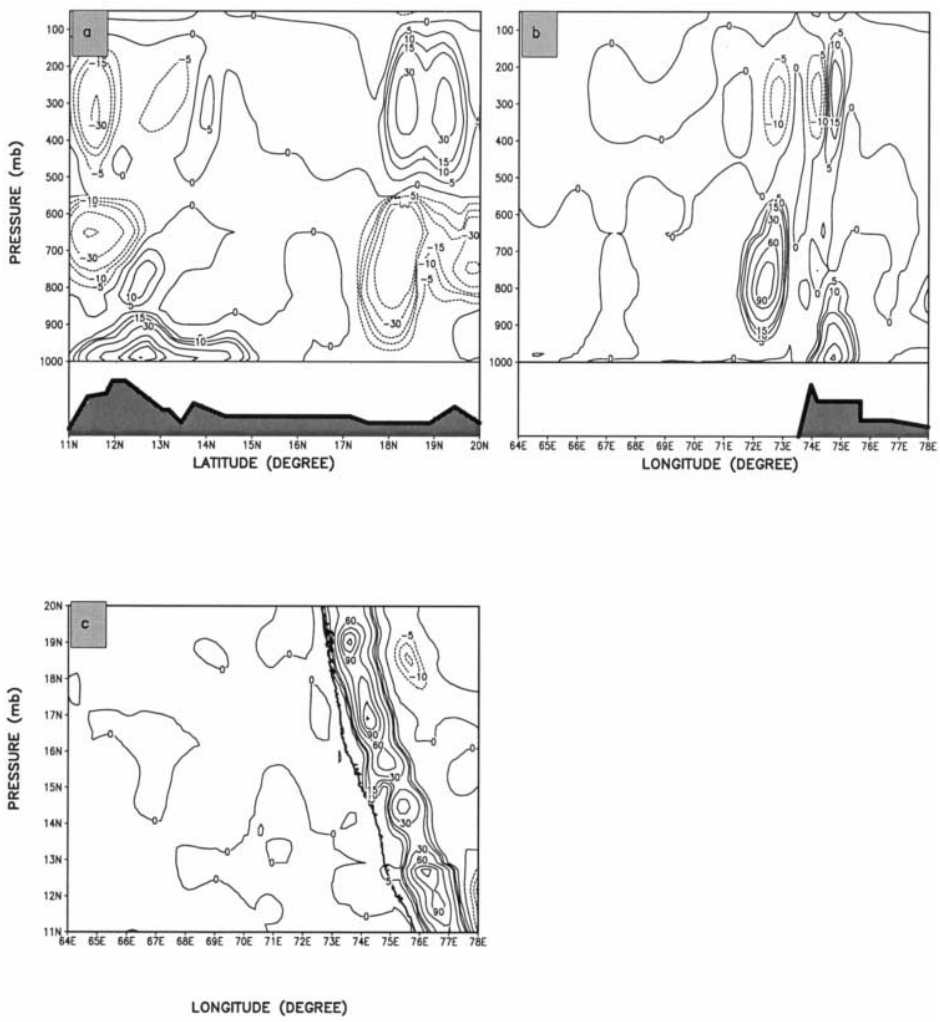

Figure 11
Simulated vertical velocities (cm s^{-1}) in the CNTRL at 36 h. (a) Latitude-height cross section at 76°E, (b) longitude-height cross section at 16°N, (c) horizontal distribution near the surface.

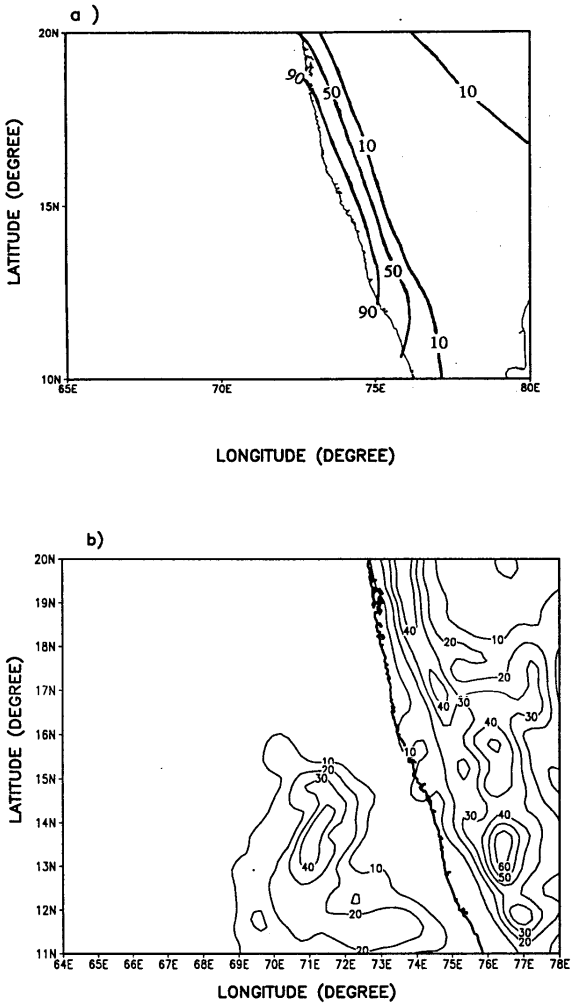

Figure 12
Rainfall fields (mm day^{-1}). (a) Observed at 0300 UTC 13 July, 1988, (b) simulated in the CNTRL at 12 h.

5.5. Rainfall over the West Coast of India

Observed and simulated rainfalls at 12 h and 36 h are displayed in Figures 12 and 13, respectively. During the southwest monsoon season, heavy rainfall occurs along the west coast of India due to the interaction of low-level flow with the WGM and offshore convections. As shown in Figure 12a, a line distribution of rainfall paralleling the west coast of India was observed on July 13, 1988. Rainfall rates decrease inland with maximum values along the shoreline. The maximum

rainfall rate is about 100 mm d^{-1}. Figure 12b shows that simulated rainfall at 12 h was located in two regions, one in the region over the Arabian Sea well off the west coast of India and the other in a region along the west coast of India. The maximum rainfall rate in the region over the Arabian Sea is larger than 40 mm d^{-1}. However, there were no observations over this region. The distribution of the simulated rainfall along the west coast of India is a line pattern with maximum values close to the shoreline. This pattern is very similar to the observations (Fig.

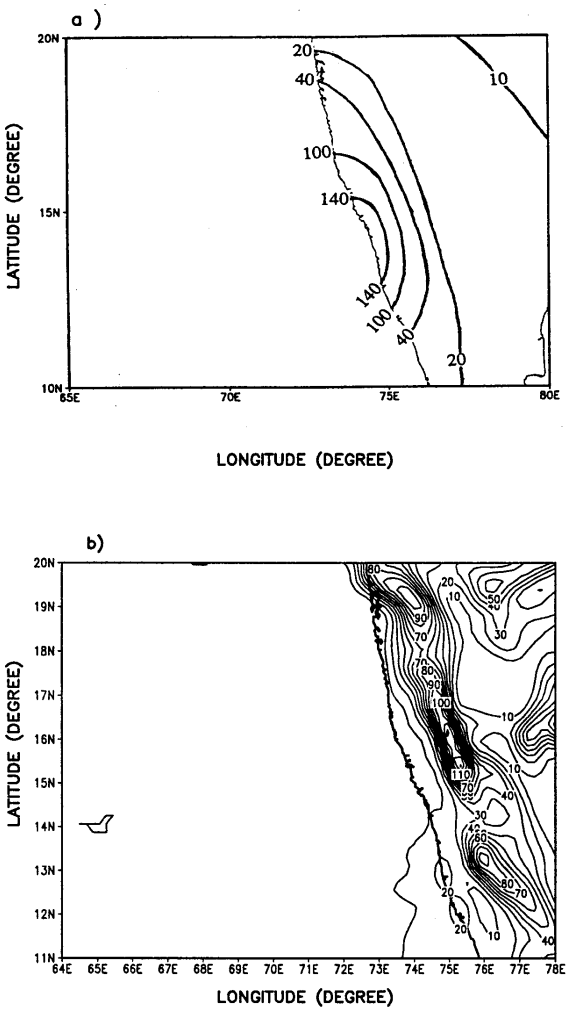

Figure 13
Rainfall fields (mm day^{-1}). (a) Observed at 0300 UTC 14 July, 1988, (b) simulated in the CNTRL at 12 h.

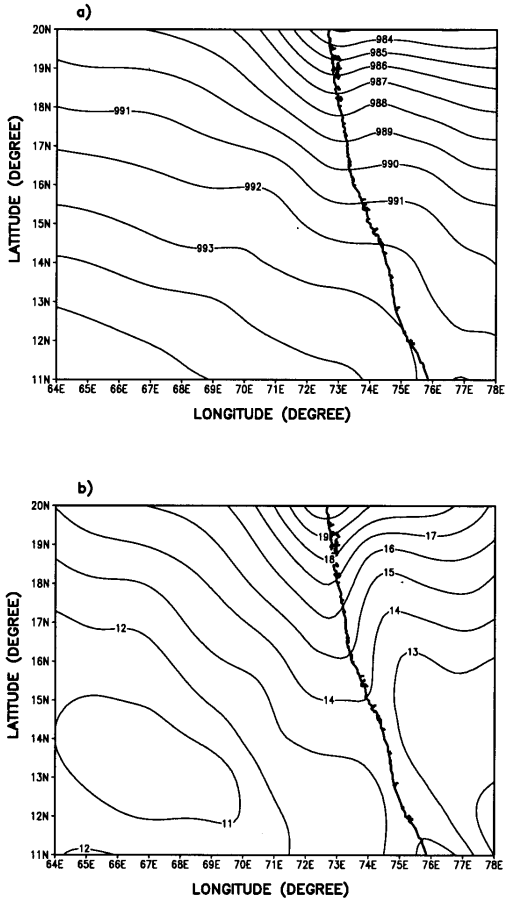

Figure 14
(a) Simulated MSP fields (mb) in the NOTOP at 12 h, (b) the difference fields (CNTRL minus NOTOP) of the MSP at 12 h.

12a). The maximum rainfall rate is larger than 60 mm d^{-1}, about 30 mm d^{-1} less as compared to the observations. Heavier rainfall along the west coast of India was observed on July 14, 1988 (Fig. 13a). The distribution pattern approaches that of the previous day with maximum values close to the shoreline. The values decrease rapidly toward inland. The maximum rainfall rate surpasses 140 mm d^{-1}. The simulated rainfall for 36 h is shown in Figure 13b. The rainfall occurs mostly along the west coast of India with some spots over the northeast region of the domain. The maximum value is larger than 120 mm d^{-1} and is located close to the shoreline. This is consistent with the observations. Note the differences between the simulated rainfall and the observations at 12 h and 36 h. These differences can be partially explained by the difference in time between the simulation and the observation, and

the coarser model terrain. The observational analysis is based on a data set without observations over the ocean and very sparse observation in the Western Ghat Mountain region. Remote sensing data (satellite and radar images) were not available for this case. However, heavy rainfall and floods are often reported in this region during monsoon periods, indicating that the model simulation produced a reasonable rainfall distribution pattern. Also, a more detailed structure of the rainfall distribution is displayed by the simulation results because of higher model resolution.

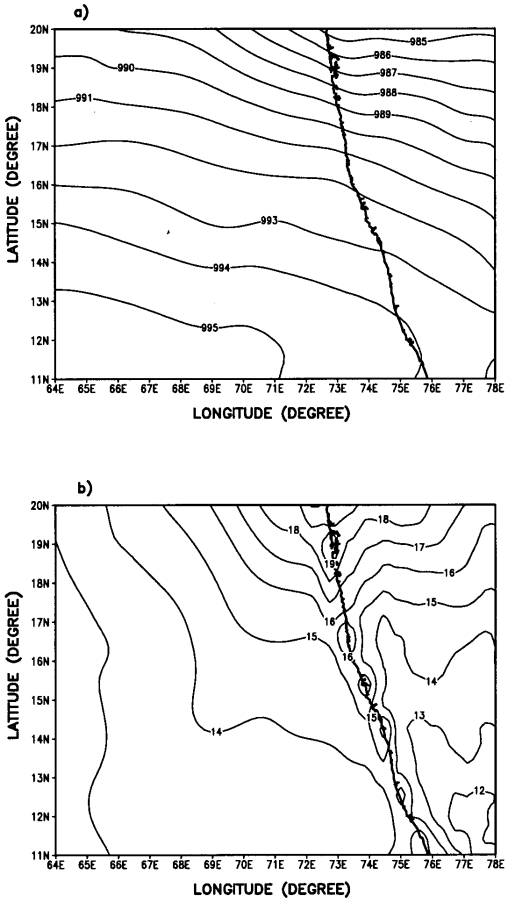

Figure 15
(a) Simulated MSP fields (mb) in the NOTOP at 36 h, (b) the difference fields (CNTRL minus NOTOP) of the MSP at 36 h.

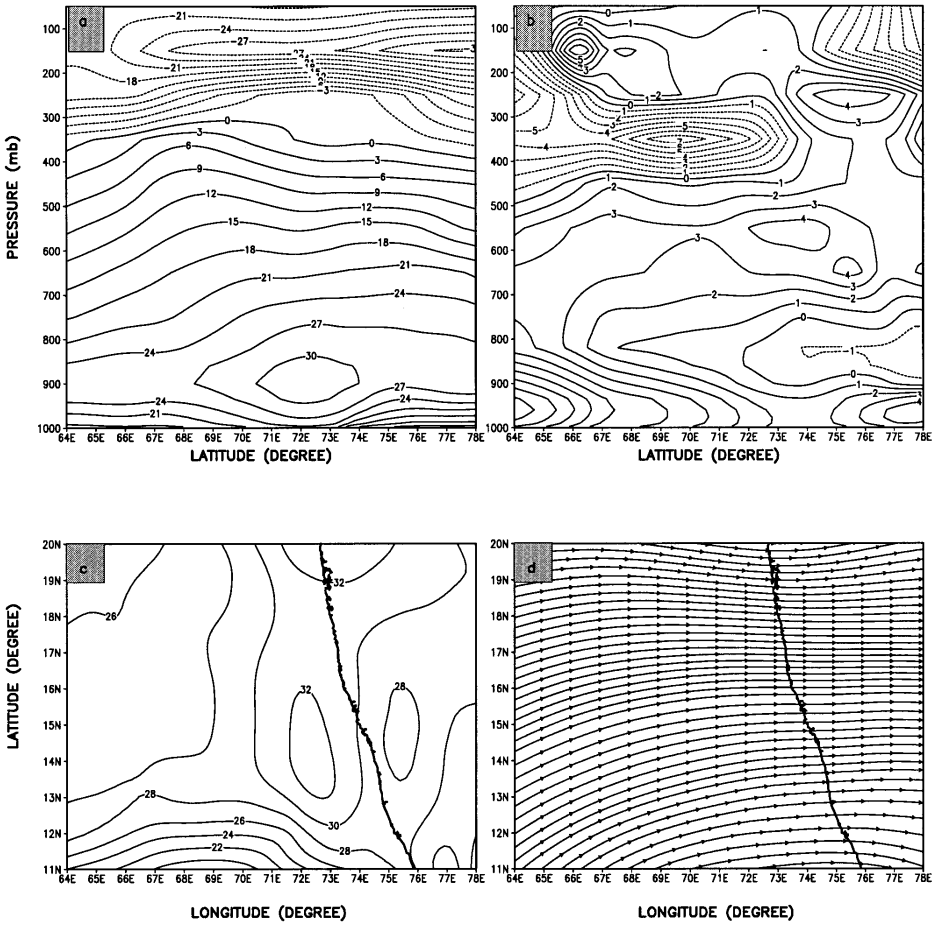

Figure 16
Simulated wind fields (m s^{-1}) in the NOTOP at 12 h. (a) Longitude-height cross section of U component at 16°N, (b) longitude-height cross section of V component at 16°N, (c) horizontal wind speed at 900 mb, (d) streamlines at 900 mb.

6. *Results of the NOTOP Run*

To investigate the effect of the WGM, a numerical experiment (NOTOP) was conducted in which the mountains were removed from the innermost model domain. However the model parameterizations and the surface characteristics, such as land use pattern and vegetation cover, are identical to those of the CNTRL run. The simulated results as well as the differences between the simulated results of the CNTRL and NOTOP runs are discussed below.

6.1. The Mean Sea-level Pressure Distribution

The simulated mean sea-level pressure (MSP) without the terrain, and the difference fields of MSP (CNTRL minus NOTOP) at 12 h and 36 h are given in Figures 14 and 15, respectively. Compared with Figure 6, two significant differences exist in panel *a* in these two figures. First, the MSP values over the whole domain are about 10 to 20 mb lower in the NOTOP run as compared to the CNTRL run. It appears that the lee side low pressure system moves upstream when the mountains are moved from the fine domain. Second, no pressure ridge was simulated along the west coast of India. Without the orography no mechanical

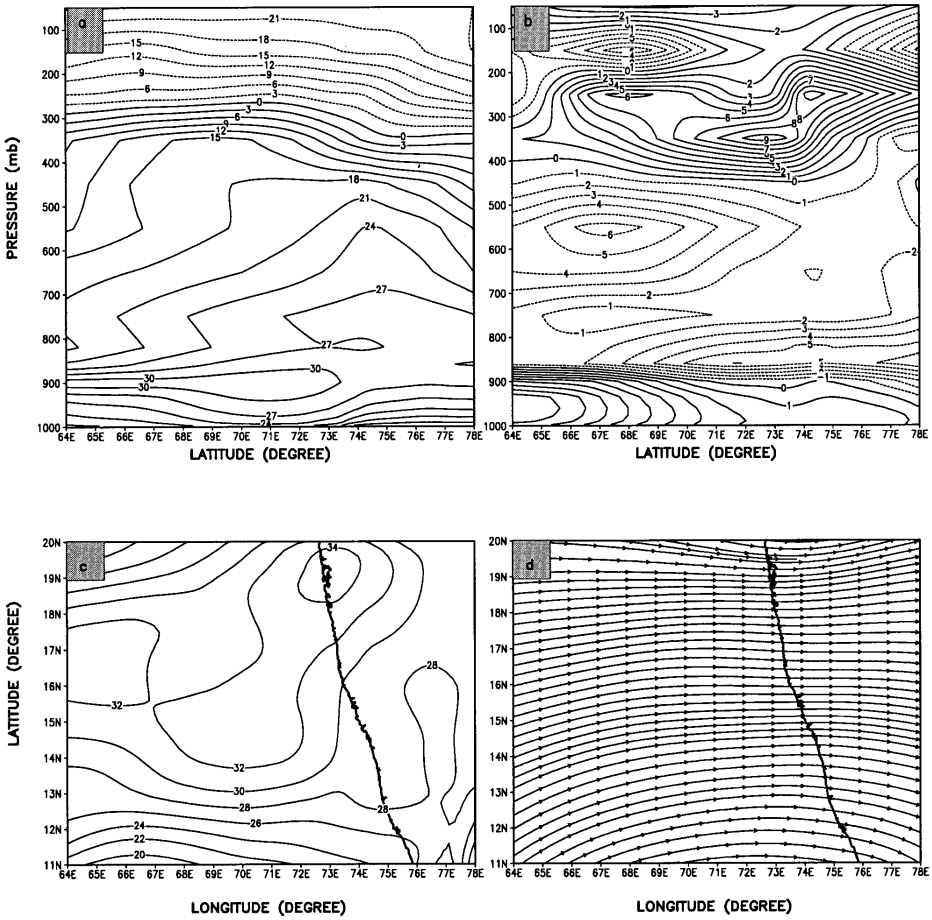

Figure 17
Simulated wind fields (m s^{-1}) in the NOTOP at 36 h. (a) Longitude-height cross section of U component at 16°N, (b) longitude-height cross section of V component at 16°N, (c) horizontal wind speed at 900 mb, (d) streamlines at 900 mb.

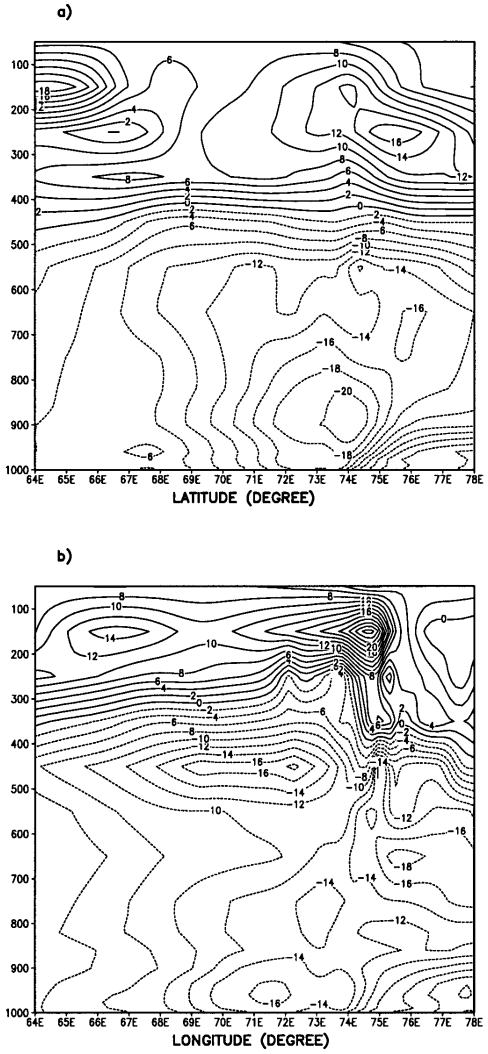

Figure 18
Longitude-height cross sections of the difference fields (CNTRL minus NOTOP) of the horizontal wind speeds (m s^{-1}). (a) 12 h, (b) 36 h.

lifting was present and hence no pressure ridge was created. The MSP differences most pronounced along the west coast of India over the northern part of the domain as shown in Figures 14b and 15b. The maximum MSP difference is about 20 mb. These results clearly demonstrate that the pressure ridge along the west coast of India arises from the blocking effect of the WGM on the low-level westerly flow.

6.2. The SLLJ

The simulated wind fields at 12 h and 36 h without the topography (Figs. 16 and 17) are very different from those with the orography (Figs. 7 and 8). As illustrated in panels *a* and *b* in Figures 16 and 17, the *U* component increases in speed while the *V* component below 900 mb does not change its sign as it does in Figures 7c and 8c as the low-level flow approaches the west coast of India. The horizontal wind speed and streamlines at 900 mb in panels *c* and *d* in these two figures indicate an increase in wind speed near the coastal region and no change in wind direction

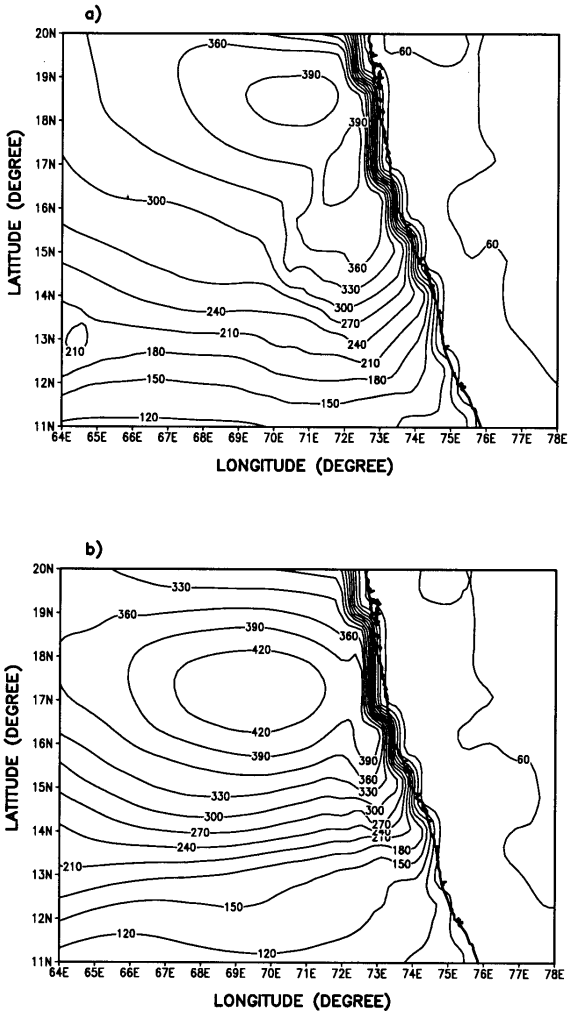

Figure 19
Simulated latent heat fluxes (W m^{-2}) in the NOTOP. (a) 12 h, (b) 36 h.

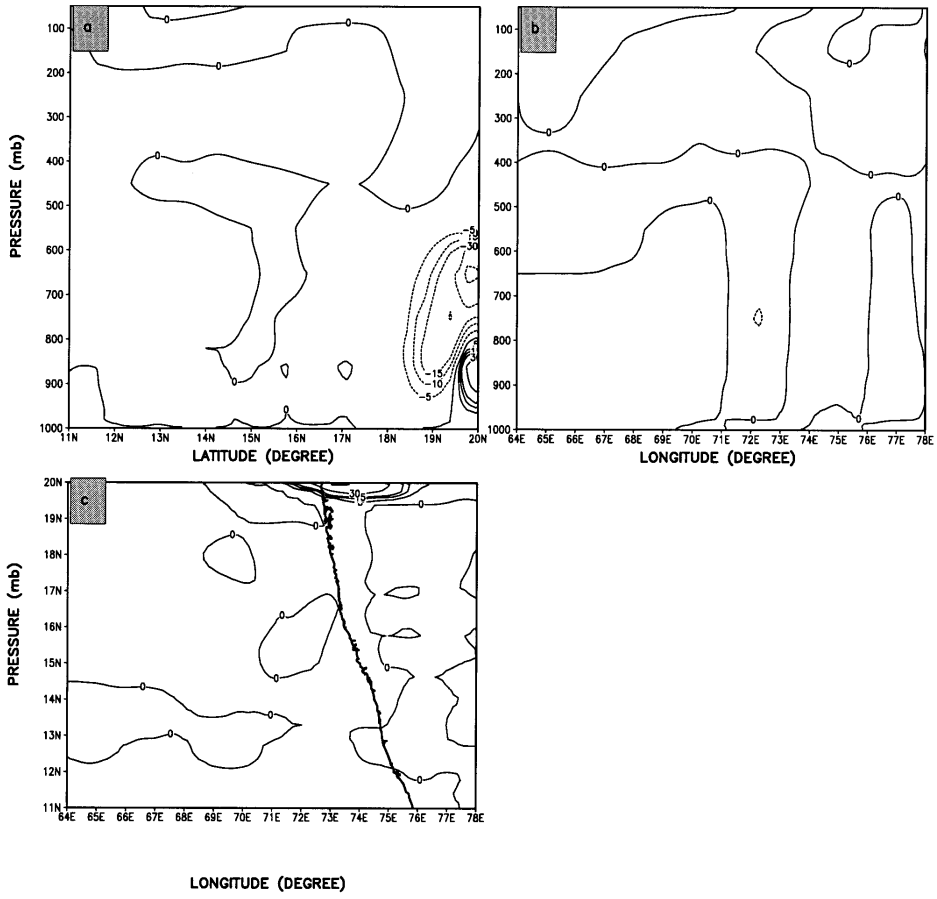

Figure 20
Simulated vertical velocities (cm s^{-1}) in the NOTOP at 12 h. (a) Latitude-height cross section at 76°E, (b) longitude-height cross section at 16°N, (c) horizontal distribution near the surface.

as the SLLJ approaches the coast. The maximum wind speed at 900 mb at both 12 h and 36 h is near the west coast of India with a value of about 34 m s^{-1}. Obviously, no deceleration and deflection occur in this case with any mountain.

As shown in panels *a* and *b* in Figures 16 and 17, the tropical easterly jets in the upper levels are considerably weaker when the mountains are removed. The vertical cross section of the difference field of (CNTRL minus NOTOP) the horizontal wind speed at 16 N is shown in Figure 18. The horizontal wind speed below 400 mb is quite stronger in the NOTOP run than in the CNTRL run while the horizontal wind speed above 400 mb is significantly weaker in the NOTOP run than in the CNTRL run. The maximum differences below and above 400 mb are about 16 to 20 m s^{-1}. The reversal zone between the low-level and the upper-level jets is located

between 400 mb and 300 mb in the NOTOP run, and about 100 mb higher than that in the CNTRL run.

6.3. Latent Heat Fluxes from the Arabian Sea

The simulated surface turbulent latent heat fluxes at 12 h and 36 h in the NOTOP run are shown in Figure 19. The distribution pattern of the latent heat flux is similar to that in the CNTRL run, with larger values over the Arabian Sea, smaller values over the land, and a strong gradient along the west coast of India. However, owing to the increase in low-level wind speed, the latent heat flux over the Arabian Sea is much stronger in this case than in the CNTRL run. The maximum

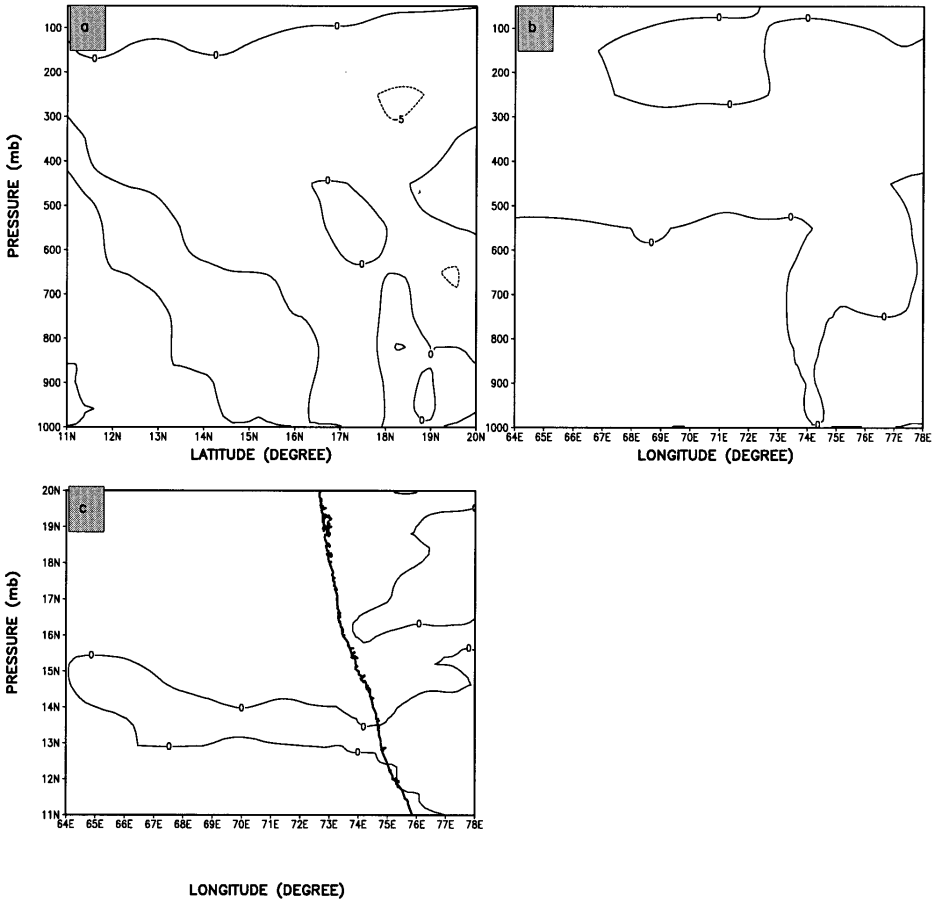

Figure 21
Simulated vertical velocities (cm s^{-1}) in the NOTOP at 36 h. (a) Latitude-height cross section at 76°E, (b) longitude-height cross section at 16°N, (c) horizontal distribution near the surface.

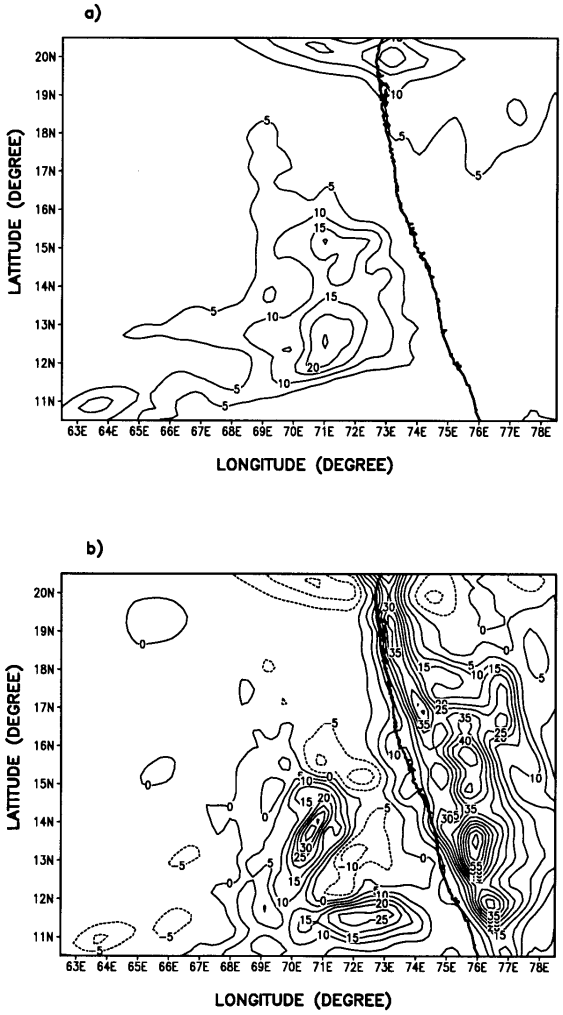

Figure 22
(a) Simulated rainfall (mm day^{-1}) in the NOTOP at 12 h, (b) the difference fields (CNTRL minus NOTOP) of rainfall at 12 h.

values at 12 h and 36 h are about 390 W m^{-2} and 420 W m^{-2}, respectively, about twice that in the CNTRL. The horizontal gradient of latent heat flux along the west coast of India is stronger in this case than that in the CNTRL run. Larger latent heat fluxes and a stronger gradient usually imply that stronger convection driven by thermal forcing occurs. This would lead to stronger vertical motions and more rainfall. However, as shown in Sections 6.4 and 6.5, very weak vertical motion and meager rainfall were simulated at both 12 h and 36 h. It appears that the thermally driven convection is suppressed by synoptic forcing. Both 12 h and 36 h correspond

to 5:30 a.m. local time. At this time, if synoptic forcing is absent, land breeze would occur near the west coast of India, i.e., the thermally driven circulation would blow from the land to the Arabian Sea. However, as shown in the previous section, strong winds are present from the Arabian Sea to the land, suppressing the local thermal circulation. Therefore, surface heating appears to be unimportant in this case.

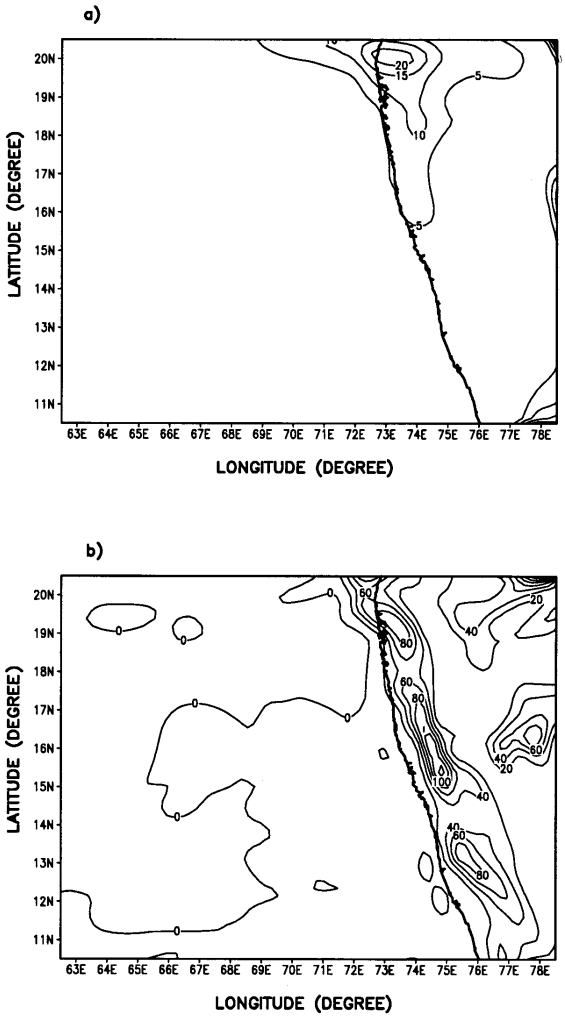

Figure 23
(a) Simulated rainfall (mm day^{-1}) in the NOTOP at 36 h, (b) the difference fields (CNTRL minus NOTOP) of rainfall at 36 h.

6.4. Vertical Motions

The simulated vertical motions at 12 h and 36 h are given in Figures 20 and 21, respectively. Very weak vertical motion was simulated in the domain at both these hours, excepting the northern boundary of the model domain where a vertical velocity exceeding 30 cm s^{-1} was simulated. Comparison between the CNTRL and the NOTOP runs indicates that stronger vertical motion simulated in the CNTRL run is the result of orographic lifting of the Western Ghat Mountains.

6.5. Rainfall

The simulated rainfall at 12 h and 36 h is given in Figures 22 and 23, respectively. At 12 h (Fig. 22a), the simulated rainfall occurs over two regions. One is along the northern boundary of the domain; and the other takes place over a wide region well off the west coast of India. Maximum values in these two regions are about 20 and 25 mm day^{-1}, respectively. These values are much less than those in the CNTRL run. No rainrall was simulated along the west coast. At 36 h (Fig. 23a), simulated rainfall is mostly distributed along the northern part of the west coast of India. The maximum value is about 20 mm day^{-1}, considerably less than that in the CNTRL run. The differences in rainfall between the two experiments (CNTRL minus NOTOP) are given in Figures 22b and 23b. Both the simulated rainfall area and the rainfall rate in the CNTRL are substantially greater than that in the NOTOP run. The maximum difference in the rainfall rates between the two experiments is about 60 mm day^{-1} at 12 h and 100 mm day^{-1} at 36 h. According to SMITH and LIN (1983), there are six theories which might account for the observed rainfall along the west coast of India: (1) smooth uplift, (2) thermal driving circulation, (3) coastal trough, (4) lifting instability, (5) low-level feeder cloud, and (6) latent heating. It seems from our simulations that (1), (4) and (6) are the major mechanisms producing strong vertical motion and heavy rainfall along the west coast of India. Smooth uplift occurs first. This produces vertical motion which leads to condensation, lifting instability and latent heating. These processes work together and create deep convection and heavy precipitation.

7. Conclusions

Two numerical experiments were performed to investigate the interaction of the SLLJ with the Western Ghat Mountains. The surface characteristics, such as land use pattern, vegetation cover, as well as the model parameterizations, are identical in the two experiments. The only difference between the two experiments is that one integrates the topography which includes mountains in the fine domain, and the other is without. Simulation of the experiment with the orography successfully

captured most of the features of the SLLJ interaction with the Western Ghat Mountains, such as a pressure ridge along the west coast, speed deceleration, and direction deflection of the low-level westerly flow west of the mountains. Other features captured are the observed strong vertical motions and heavy rainfall along the west coast of India. The results from the experiment without the orography failed to reproduce these features. The comparison between the two experiments suggests that during the India summer monsoon season, the major influence of the Western Ghat Mountains on the low-level westerly flow from the Arabian Sea results from blocking and deflection, indicating that the rainfall along the west coast of India is primarily caused by the orographic lifting of the air parcels which causes instability and enhanced latent heating at upper levels, thus triggering deep convection in this region.

8. Acknowledgments

This work was supported by the Naval Research Laboratory, Atmospheric Sciences Division of the National Science Foundation and the Department of Energy under Contract 091575-A-Q1 with Pacific Northwest Laboratories. The computation for this work was performed at the North Carolina Supercomputing Center, Research Triangle Park. The authors would like to thank Dr. Yuh-lang Lin and Dr. R. V. Madala for several helpful discussions. Ms. Elena Pietrafesa provided assistance in editing the manuscript.

References

ANTHES, R. A. (1977), *A Cumulus Parameterization Scheme Utilizing a One-dimensional Cloud Model*, Mon. Wea. Rea. *105*, 207–286.

CHEN, T., and LOON, H. V. (1987), *Interannual Variation of the Tropical Easterly Jet*, Mon. Wea. Rev. *115*, 1739–1759.

DAS, P. K., *The Monsoon* (St. Martin's Press Inc., New York 1972).

DAVIES, H. C. (1976), *A Lateral Boundary Formulation for Multi-level Prediction Models*, Q. J. R. Meteorol. Soc. *102*, 405–418.

DAVIES, H. C. (1983), *Limitations of Some Common Lateral Boundary Schemes Used in Regional NWP Models*, Mon. Wea. Rev. *111*, 1002–1012.

FEIN, J. S., and STEPHENS, P. L., *Monsoons* (John Wiley and Sons, Inc., New York 1987).

GROSSMAN, R. L., and DURRAN, D. R. (1984), *Interaction of Low-level Flow with the Western Ghat Mountains and Offshore Convection in the Summer Monsoon*, Mon. Wea. Rev. *112*, 652–672.

HOLT, T., and RAMAN, S. (1986), *Variation of Turbulence in the Marine Boundary Layer over Arabian Sea during Indian Southwest Monsoon (MONEX 79)*, Boundary Layer Meteor. *37*, 71–87.

HOLT, T., and RAMAN, S. (1987), *A Study of Mean Boundary-layer Structures over the Arabian Sea and the Bay of Bengal during Active and Break Monsoon Periods*, Boundary Layer Meteor. *38*, 73–94.

HOLT, T., and RAMAN, S. (1988), *A Review and Comparative Evaluation of Multilevel Boundary-layer Parameterizations for First-order and Turbulent Kinetic Energy Closure Schemes*, Rev. Geophys. *26*, 761–780.

HOLT, T., CHANG, S., and RAMAN, S. (1990), *A Numerical Study of the Coastal Cyclogenesis in GALE IOP 2; Sensitivity to PBL Parameterization*, Mon. Wea. Rev. *118*, 234–257.

KRISHNAMURTI, T. N. (1971), *Tropical East–west Circulation during the Northern Summer*, J. Atmos. Sci. *28*, 1342–1347.

KRISHNAMURTI, T. N., COCKE, S., PASCH, R., and LOW-NAM, S. (1983), *Precipitation Estimates from Raingauge and Satellite Observations: Summer MONEX*, Dept. of Meteorology, Florida State University, 377 pp.

KUO, H. L. (1974), *Further Studies of the Parameterization of the Influence of Cumulus Convection on Large-scale Flow*, J. Atmos. Sci. *31*, 1232–1240.

MADALA, R. V., CHANG, S. W., MOHANTY, U. C., MADAN, S. C., PALIWAL, R. K., SARIN, V. B., HOLT, T., and RAMAN, S. (1987), *Description of the NAVA Research Laboratory Limited Area Dynamical Weather Prediction Model*, NRL Memo. Rep. *5992*, Naval Research Laboratory, Washington, D.C.

MONIN, A. S., and YAGLOM, A. M., *Statistical Fluid Mechanics* (MIT Press, Cambridge, MA 1971) Vol. 1, pp. 468–504.

NOILHAN, J., and PLANTON, S. (1989), *A Simple Parameterization of Land-surface Processes for Meteorological Models*, Mon. Wea. Rev. *117*, 536–549.

OGURA, Y., and YOSHIZAKI, M. (1988), *Numerical Study of Orographic-convective Precipitation over the Eastern Arabian Sea and the Ghat Mountains during the Summer Monsoon*, J. Atmos. Sci. *45*, 2097–2122.

RAMAGE, C. S., *Monsoon Meteorology* (Academic Press, New York 1971).

SARKER, R. P., SINHA, K. C., and DE, U. S. (1978), *Dynamics of Orographic Rainfall*, Indian J. Met. Hydrol. Geophys. *29*, 335–348.

SASHEGYI, K. D., and MADALA, R. V. (1993), *Application of Vertical-mode Initialization to a Limited-area Model in Flux Form*, Mon. Wea. Rev. *121*, 207–220.

SMITH, R. B., and LIN, Y. (1983), *Orographic Rain on the Western Ghat*. In *Proceedings First Sino-American Workshop on Mountain Meteorology* (E. R. Reiter, Z. Baozhen, and Q. Yongfu, eds.) pp. 71–94.

SMITH, R. B. (1985), *Comment on "Interaction of Low-level Flow with the Western Ghat Mountains and Offshore Convection in the Summer Monsoon,"* Mon. Wea. Rev. *113*, 2176–2177.

VAN DE BOOGGARD, H. (1977), *The Mean Circulation of the Tropical and Subtropical Atmosphere—July*, NCAR Tech. Note, NCAR/TN-118 + STR, National Center for Atmospheric Research, 48 pp.

(Received September 4, 1998, accepted December 9, 1998)